Deployable Sandwich Surfaces with High Out-of-Plane Stiffness

Evgueni T. Filipov, A.M.ASCE[1]; Glaucio H. Paulino, M.ASCE[2]; and Tomohiro Tachi[3]

Abstract: This paper presents a set of deployable origami tube structures that can create smooth functional surfaces while simultaneously maintaining a high out-of-plane stiffness both during and after deployment. First, a generalized geometric definition for these tubes is presented such that they can globally have straight, curved, or segmented profiles, while the tubes can locally have skewed and reconfigurable cross sections. Multiple tubes can be stacked to form continuous and smooth assemblies in order to enable applications, including driving surfaces, roofs, walls, and structural hulls. Three-point bending analyses and physical prototypes were used to explore how the orthogonal stiffness of the tubular structures depends on the geometric design parameters. The coupled tube structures typically had their highest out-of-plane stiffness when near to a fully deployed state. Tubes with skewed cross sections and more longitudinal variation (i.e., that had more zigzags) typically had a higher stiffness during deployment than tubes that were generally straight. **DOI: 10.1061/(ASCE)ST.1943-541X.0002240.** © *2018 American Society of Civil Engineers.*

Author keywords: Deployable structures; High stiffness; Origami; Coupled tubes.

Introduction

Over the last several decades origami has transitioned from art to scientific research and more recently to engineering technologies, ranging from medical devices (Randall et al. 2012) to everyday consumer products (Morris et al. 2016). The benefits of origami include the capability for self-assembly from a flat state, deployment from a stowed configuration, reconfiguration for multifunctionality, adaptable physical properties, and more. Within civil engineering and architecture, origami principles have been used to conceive system components such as adaptable surfaces and facades [e.g., Del Grosso and Basso (2010) and Thün et al. (2012)] to full, large-scale, deployable structures [e.g., Tachi et al. (2012), Cai et al. (2015), and Ballard et al. (2016)]. Despite the potential benefits of using origami in large-scale applications, there have been few practical implementations, and there are still many challenges that prevent commercialization.

A fundamental challenge has been the need to use thin panels, which allow compact packing and reconfiguration, while at the same time preserving structural stiffness and rigidity, which conversely requires thick panels. To overcome this challenge, many origami structures use a cellular or sandwich design that intentionally locks thin sheets into an overconstrained system after deployment [e.g., Schenk and Guest (2013), Martínez-Martín and Thrall (2014), Gattas and You (2015), and Gattas et al. (2017)]. One issue with this approach is that the structures are flexible and possibly unstable during assembly and deployment. Some of these systems are also inherently flexible, because they allow deformation motions where bending and folding of the panels occur, even in a deployed and locked state. To overcome this challenge, our work uses a zipper coupling approach for origami tubes previously introduced by the authors (Filipov et al. 2015). These structures do not require complex locking mechanisms and only need to be affixed at the ends in order to prevent global motion with bending and folding.

An additional drawback for origami designs has been that they are segmented and result in sawtoothlike structures [e.g., Cai et al. (2015), Filipov et al. (2015), and Lee and Gattas (2016)] that cannot be readily utilized in applications for which a smooth surface is required. Such applications in civil engineering include roadways, roofs, walls, and formwork. In other engineering applications such as hulls, wings, and waterways, nonsmooth origami could lead to complex and unwanted fluid structure interaction. The geometries explored in this paper are based on fundamental variations of zipper tubes that fall into a category of cylindrical generating surfaces with mirror-symmetric walls. These systems were introduced by the authors in Tachi et al. (2015) but were not explored in detail. These folding systems can provide both aesthetic design and functional purpose, such as the concept for a deployable canopy shown in Fig. 1. The system has a smooth surface when deployed but a nonstraight profile similar to an architectural canopy. Moreover, the zipper-coupled sandwich geometry enhances the out-of-plane stiffness both during deployment and in the final state.

More practical challenges for implementing origami designs on a large-scale include system design (e.g., panels connected with hinges versus thin sheets with large strains at folds) and the corresponding material systems (e.g., metals, polymers, composites). The systems need to allow kinematic motion but also provide strength and stiffness for the structure. Our work does not address these challenges; however, the proposed overall system does provide advantages for practical implementation. The coupled origami tubes use a concept of rigid folding in which the panels remain flat and deformations are localized at the fold lines. This folding technique allows for thickness to be incorporated with practical materials and discrete, hinge-based designs. Furthermore the sandwich

[1]Assistant Professor, Dept. of Civil and Environmental Engineering, Univ. of Michigan, 2350 Hayward St., Ann Arbor, MI 48109 (corresponding author). Email: filipov@umich.edu

[2]Raymond Allen Jones Chair, School of Civil and Environmental Engineering, Georgia Institute of Technology, 790 Atlantic Dr. NW, Atlanta, GA 30332. Email: paulino@gatech.edu

[3]Associate Professor, Graduate School of Arts and Sciences, Univ. of Tokyo, 3-8-1 Komaba, Meguro-Ku, Tokyo 153-8902, Japan. Email: tachi@idea.c.u-tokyo.ac.jp

Note. This manuscript was submitted on September 14, 2017; approved on July 11, 2018; published online on November 28, 2018. Discussion period open until April 28, 2019; separate discussions must be submitted for individual papers. This paper is part of the ***Journal of Structural Engineering***, © ASCE, ISSN 0733-9445.

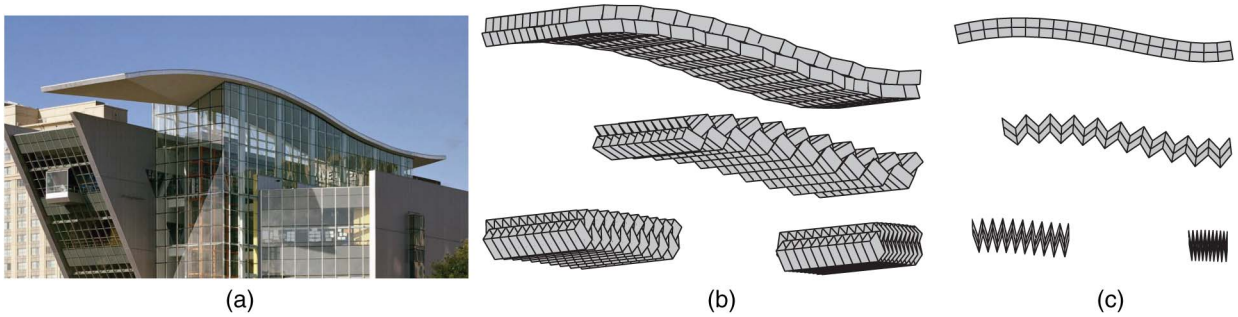

Fig. 1. Canopy structures: (a) roof of the Connecticut Science Center by César Pelli & Associates (reprinted from Woodruff and Brown 2009, with permission). Deployment sequence of a curved canopy constructed with zipper-coupled origami tubes shown in (b) isometric; and (c) side views.

cell geometry of the coupled tubes makes the systems stiffer, allowing for the use of thinner and more flexible materials.

Generalized Projection Definition for Quadrilateral Origami Tubes

A simplified projection-based technique was used to define the geometry of the origami tubes. In this paper, the tubes are created only with rhombus cross sections (four equal edges), although the techniques presented here can be used with any parallelogram cross section. The projection methodologies can also be used on tubes with arbitrary polygonal cross sections; however, polygonal tubes may restrict some of the folding characteristics [see Filipov et al. (2016)].

To construct a quadrilateral origami tube, we start by constructing a rhombus cross section in the Y, Z-plane. The bottom of the cross section is parallel with the Y-axis, and an angle θ counterclockwise from the Z-axis defines the rhombus. Next, two angles ϕ_Y and ϕ_Z are used to guide the direction of projection, from the X-axis toward the Y- and Z-axes, respectively (Fig. 2).

Straight Origami Tubes

For a straight tube, we project the cross section in the X-direction onto a projection plane that is parallel to the Y, Z-plane. A segment length parameter l_i that lies only in the X, Z-plane defines the distance between the ith and the $i+1$th projection planes. Thus, the distance between projection planes in the X-direction can be calculated as $l_i \cos(\phi_Z)$. This definition is subsequently important for the coupling of multiple tubes.

The projection creates a new rhombus cross section that is parallel with the initial cross section. The corresponding edges of the cross sections are connected with thin origami sheets, creating a system of fold lines and panels. At the subsequent projection plane, the tube is mirrored locally; in other words, the opposite projection angles are used for the subsequent projection ($-\phi_Y$ and $-\phi_Z$). This mirroring ensures the flat foldability of the origami tube, which means that the system can theoretically fold flat into a two dimensional state. For subsequent discussion, we define top/bottom folds to be those that are symmetric to the Y-axis, while side folds are those that are rotated θ from the Z-axis (Fig. 2).

When a square cross section is used and the angles ϕ_Y and ϕ_Z are equal $(\phi = \phi_Y = \phi_Z)$, this projection approach generates a symmetric and partially developable Miura-ori tube. The tube is partially developable, because it has portions that can be created by folding an initially flat sheet. The projection approach is nonunique, and the same tube can be constructed by using different sets of parameters. For example, a rhombus cross section for which $\theta \neq 0$ and $\phi_Y \neq \phi_Z$ could also be used to create a partially developable tube but in a different folded configuration (see the kinematics of the tubes in the following section).

Curved (Nonstraight) Origami Tubes

Projection planes do not need to be parallel, and it is possible to create a variety of curved (or nonstraight) origami tube structures in three dimensions (Tachi et al. 2015; Filipov et al. 2016).

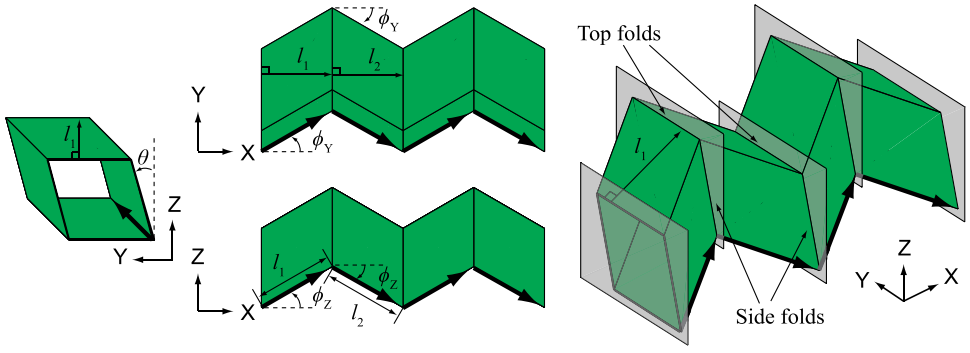

Fig. 2. Generalized projection approach to define a straight tube inspired by the Miura-ori pattern. The tube is constructed by starting with a cross section in the Y, Z-plane and projecting the cross section in the X-direction. The rhombus cross section has unit (1) dimensions and is defined by an angle θ. The projection is guided by the angles ϕ_Y and ϕ_Z with respect to the X-axis. The cross section is projected by a distance l_i in the X, Z-plane. The tube in this figure has dimensions of $\phi_Y = 30°$, $\phi_Z = 30°$, $\theta = 15°$, and $l_1 = l_2 = l_i = 1$.

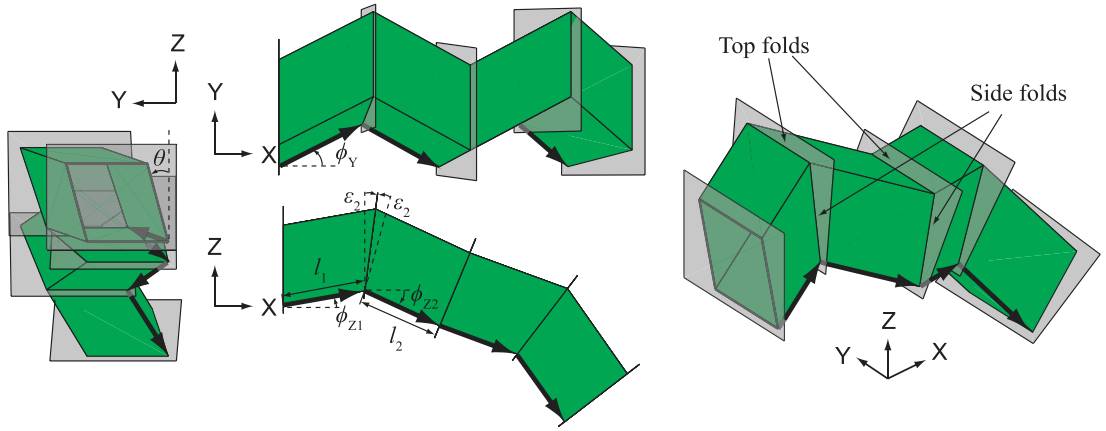

Fig. 3. Generalized projection approach to define a curved (nonstraight) tube. The tube is constructed by starting with a cross section in the Y, Z-plane and projecting the cross section in the X-direction. Subsequent projection planes can be rotated in the X, Z-plane by an angle ϵ. The distance between projection planes l_i is measured along the bottom of the tube in the X, Z-plane. The tube in this figure has dimensions of $\phi_Y = 30°$, $\phi_{Z1} = 10°$, $\theta = 15°$, $\epsilon_2 = \epsilon_3 = \epsilon_i = 7.5°$, and $l_1 = l_2 = l_i = 1$.

To facilitate the coupling of tubes, the curvature of the tubes in this paper was limited to rotating the projection planes in the X, Z-plane. Fig. 3 shows a tube in which the ith projection plane is rotated in the X, Z-plane by an angle ε_i. The rotation occurs about the bottom of the newly projected bottom edge of the cross section. In other words, the bottom edge of the cross section is translated by $l_i \cos(\phi_{Zi})$ in the X-direction and $l_i \sin(\phi_{Zi})$ in the Z-direction, and the projection plane is rotated about this new line. The tube is again mirrored locally about the projection plane, and the projection angle ϕ_Z is updated based on the projection plane rotation, e.g., $\phi_{Z2} = \phi_{Z1} + 2\varepsilon_2$. The symmetry imposed by mirroring ensures flat foldability and rigid folding kinematics.

Coupling of Two Tubes

The generalized projection scheme can be used to construct tubes that are connected along common coupling surfaces. For clarity, this section, and most of the paper is limited to the coupling of two tubes, which are designated as top (T) and bottom (B) tubes depending on their location in the Z-direction. Fig. 4 shows a schematic of two tubes that were generated using the same cross section and projection technique discussed previously. The two tubes follow the same coupling surface defined by the projection in the X, Z-direction; however, it is possible for the tubes to have different cross sections and different Y-projections. The Y-projections are defined by ϕ_{YT} and ϕ_{YB}, while the cross section rotations are defined by θ_T and θ_B for the top and bottom tubes, respectively. The angles ϕ_Y and θ are measured counterclockwise from the X- and Z-axes, respectively. With this definition, the bottom tube shown in Fig. 4 has a negative ϕ_{YB} and a negative θ_B.

The definitions can be extended as described previously, with the segment length l_i varied at different segments, as long as l_i is measured at the coupling surface and is the same for both tubes. Changing the segment length does not affect the foldability of the tube. The coupled tubes can be made curved, similar to Fig. 3, in which an angle ϵ_i was used to rotate the projection plane for both tubes. For nonstraight zipper-coupled tubes (i.e., $\epsilon_i \neq 0°$) to be valid and foldable, ϕ_{YT} must equal $-\phi_{YB}$, and θ_T must

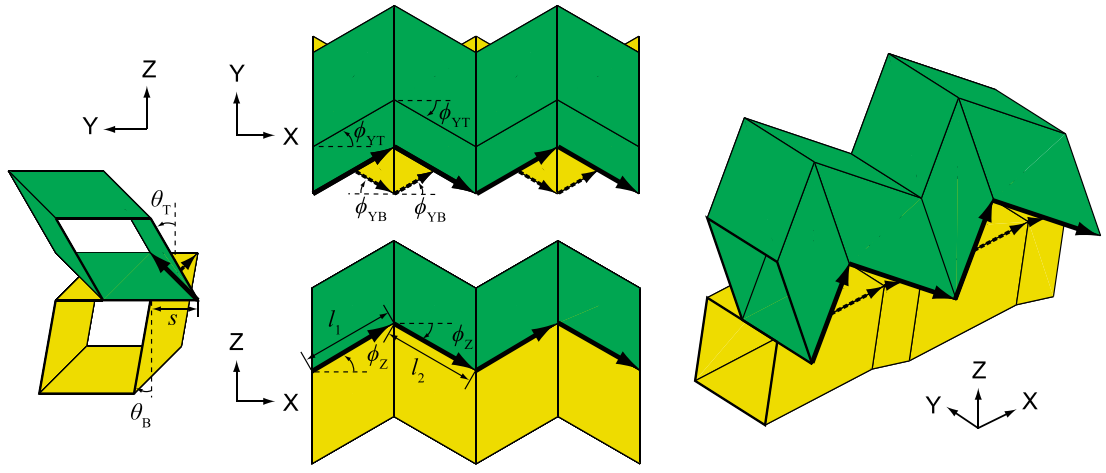

Fig. 4. Geometric definition of a zipper-coupled tube system. Two separate tubes are constructed by projecting the cross section in the X-direction. The top (T) and bottom (B) tubes can have different projection angles in the Y-direction (ϕ_{YT} and ϕ_{YB}) and can also have different cross sections (θ_T and θ_B). The two tubes must have the same projection characteristics in the Z, X-plane (angles ϕ_Z and lengths l_i). The zipper tube system in this figure has dimensions of $\phi_{YT} = 30°$, $\phi_{YB} = -30°$, $\phi_Z = 30°$, $\theta_T = 30°$, $\theta_B = -10°$, and $l_1 = l_2 = l_i = 1$.

equal $-\theta_B$. The other alternative is an aligned coupled system in which $\phi_{YT} = \phi_{YB}$ and $\theta_T = \theta_B$. The reason for these restrictions as they relate to the kinematics and foldability are discussed in the next section.

Folding Kinematics of Tube Variations

Origami patterns with four folds per vertex are one degree of freedom (one-DOF) folding mechanisms, in which the entire folded geometry of the folds and panels can be calculated from a single variable, such as one of the fold angles (Hull 2012). In a generic case, when additional and arbitrary constraints are added, the system becomes an overconstrained mechanism and is no longer rigidly foldable. However, there are ways to incorporate additional components (and constraints) such that the origami system maintains the one-DOF rigid folding mechanism: (1) origami patterns such as the Miura-ori use repetition to connect multiple one-DOF vertices into a system that preserves rigid foldability [e.g., Miura (2009) and Gattas et al. (2013)]; (2) more advanced origami structures such as the Miura-ori tube use symmetry to connect multiple patterns together while simultaneously maintaining the one-DOF folding mechanism [e.g., Tachi (2009) and Miura and Tachi (2010)]; and (3) furthermore, the coupling of two or more identical or compatible tubes also preserves the folding properties [e.g., Cheung et al. (2014) and Filipov et al. (2015)]. However, the coupling of tubes and adding compatible components to origami systems is generally not a trivial task.

In Tachi et al. (2015), we explored the two basic geometric families of allowable coupling methods for rigid foldable origami tubes. These families allow for compatibility between the coupled structures and permit the rigid folding motion. The two families are (1) coupling on an arbitrary straight or curved surface where the fold lines are parallel and mirroring is used between the bottom and top tubes to ensure rigid foldability; and (2) coupling on a flat developable surface with nonsymmetric fold lines, with arbitrary fold angles calculated to preserve rigid folding motion (Tachi et al. 2015). The generalized approach used in this paper makes use of the first family; we use an arbitrary coupling surface (defined by ϕ_Z and ϵ). We then enforce symmetry on the top and bottom of the structure by limiting the cross section and projection variations (i.e., $\phi_{YT} = -\phi_{YB}$ and $\theta_T = -\theta_B$).

Reconfiguration Kinematics of Single Tubes

The folding kinematics and reconfiguration of the coupled systems are directly related to the characteristics of each of the two (or more) coupled tubes. It is useful to first investigate the individual tubes to understand how the geometric definitions affect the global kinematics. Fig. 5 shows the kinematics of four origami tubes with different projection angles and cross sections. When a square cross section is used with $\phi_Y = \phi_Z$, we create a partially developable tube that can fold into a fully deployed, flat state in the X, Y-axis [bottom right of Fig. 5(a)]. This tube has only one folding sequence that preserves the tubular shape. Tube variations created with the projection methodology that are not partially developable cannot reach a flat state in the X, Y-plane [Fig. 5(b–d)]. However, these nonpartially developable tubes are reconfigurable because they can extend and retract through two distinct motions.

Origami tubes with square cross sections and $\phi_Z < \phi_Y$ reconfigure when the top and bottom surfaces reach a flattened state. The top and bottom folds of the tube experience switching where the mountain folds turn to valleys and vice versa [Fig. 5(b)]. However, tubes with square cross sections and $\phi_Z > \phi_Y$ reconfigure with the

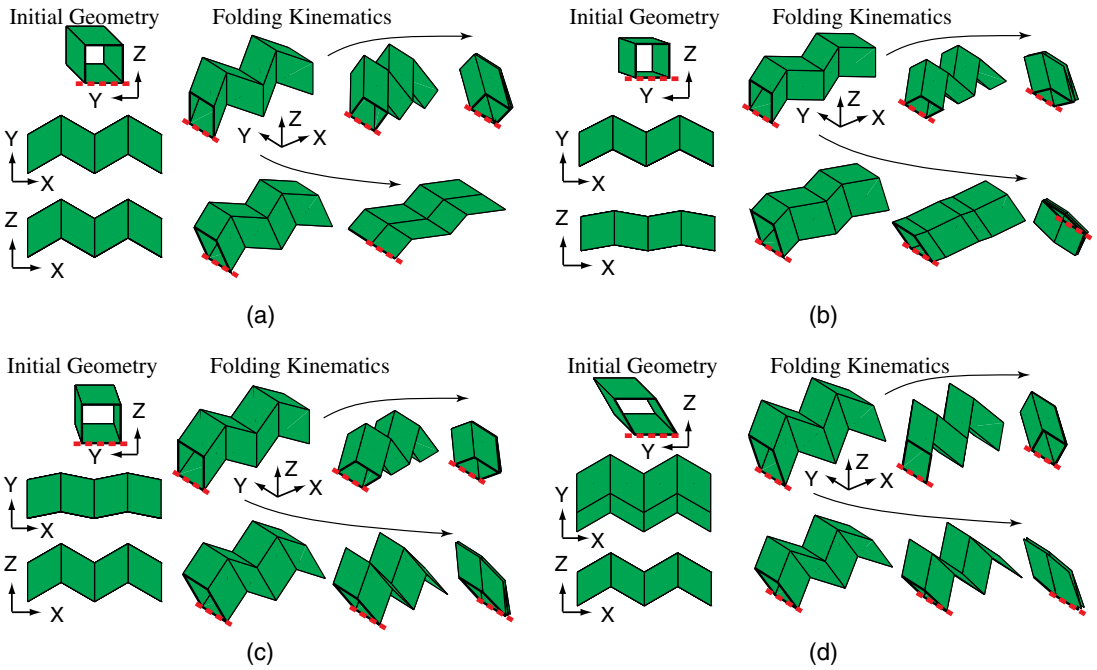

Fig. 5. Initial geometries and folding kinematics of different rigid foldable tubes. A thick dotted line parallel to the Y-axis is shown as a reference for all configurations: (a) tube created with $\phi_Z = \phi_Y = 30°$ and a square cross section; (b) tube with $\phi_Z = 10° < \phi_Y = 30°$; the tube reconfigures when the folds on the top and bottom surfaces change from mountain to valley folds; (c) tube with $\phi_Z = 30° > \phi_Y = 10°$; the tube reconfigures when the folds on the sides change from mountain to valley folds; and (d) tube with $\phi_Z = \phi_Y = 30°$ and a rhombus cross section ($\theta = 30°$); this tube follows kinematics similar to (c). The tube in (a) is partially developable and flat foldable. The tubes in (b)–(d) are not partially developable, but are flat foldable and can fold down through two different kinematic motions.

J. Struct. Eng., 2019, 145(2): 04018244

side fold lines switching [Fig. 5(c)]. Changing the cross section also influences the global kinematics in similar ways, with an increase in θ tending toward side folds switching [Fig. 5(d)], and a decrease in θ tending toward top/bottom folds switching. The projection and cross section effects can counteract each other, and it is possible to construct a partially developable tube with $\phi_Z < \phi_Y$ and $\theta > 0$. For example, one of the folded configurations in Fig. 5(a) could be the initial geometry of a tube (defined with $\phi_Z < \phi_Y$ and $\theta > 0$).

Reconfiguration Kinematics of Coupled Tubes

When two tubes are coupled, it is possible to have different types of reconfiguration occur, with either one or both of the tubes reconfiguring. The deployment sequence and kinematic properties are determined by the geometry of each tube's projection and cross section. Reconfiguration of coupled tubes follows many of the same characteristics as those shown in Fig. 5. If we assume that the cross sections of both tubes are square, then possible reconfiguration kinematics can be grouped into four categories:

- No switching: $\phi_Z = \phi_{YT} = -\phi_{YB}$: When all projection angles are equivalent (or negative and equal magnitude) both tubes are partially developable and the system can reach a flat state in the X, Z-plane [as in Fig. 5(a)].
- Top/bottom folds switch: $\phi_Z < \min(\phi_{YT}, -\phi_{YB})$: If the Z-projection is the smallest of the three, then the top and bottom folds of both tubes reconfigure [Fig. 6(a)].
- Side folds of one tube switch: $\phi_{YT} < \min(\phi_Z, -\phi_{YB})$ or $-\phi_{YB} < \min(\phi_Z, \phi_{YT})$: If one tube has a Y-projection smaller than the Z-projection, the side folds of the tube with the smallest Y-projection will reconfigure [Fig. 6(b)].
- Side folds of both tubes switch: $\phi_{YT} = \phi_{YB} < \phi_Z$: Both tubes have equivalent Y-projection angles (or negative and equal magnitude), and each tube can reconfigure independently at its side folds when the system reaches a fully deployed state.

The kinematics of two common coupled tube cases are shown in Fig. 6. When the cross sections are changed into rhombuses, the switching cases remain the same as in the aforementioned four cases, but the projection angles alone do not determine the case. For tubes that have curvature, it is possible to have multiple cases occur over the length of the tube. The tube shown in Fig. 6(a) has a curve with all top and bottom folds reconfiguring simultaneously. If the curvature of the system is varied, it is possible that only one portion of the fold lines will flatten, and the structure will have only one folding motion (no switching can occur).

Systems of Coupled Tubes

Coupling of tubes can be further extended to create continuous and more complex deployable systems. The primary method for coupling discussed herein uses a projection technique and a common coupling surface to couple tubes (zipper-type coupling). The projection-based coupling technique is generalized and can allow for the coupling of curved tubes and the coupling of straight tubes with different cross-sectional geometries. However, the projection-based technique is partially limiting, because it can only

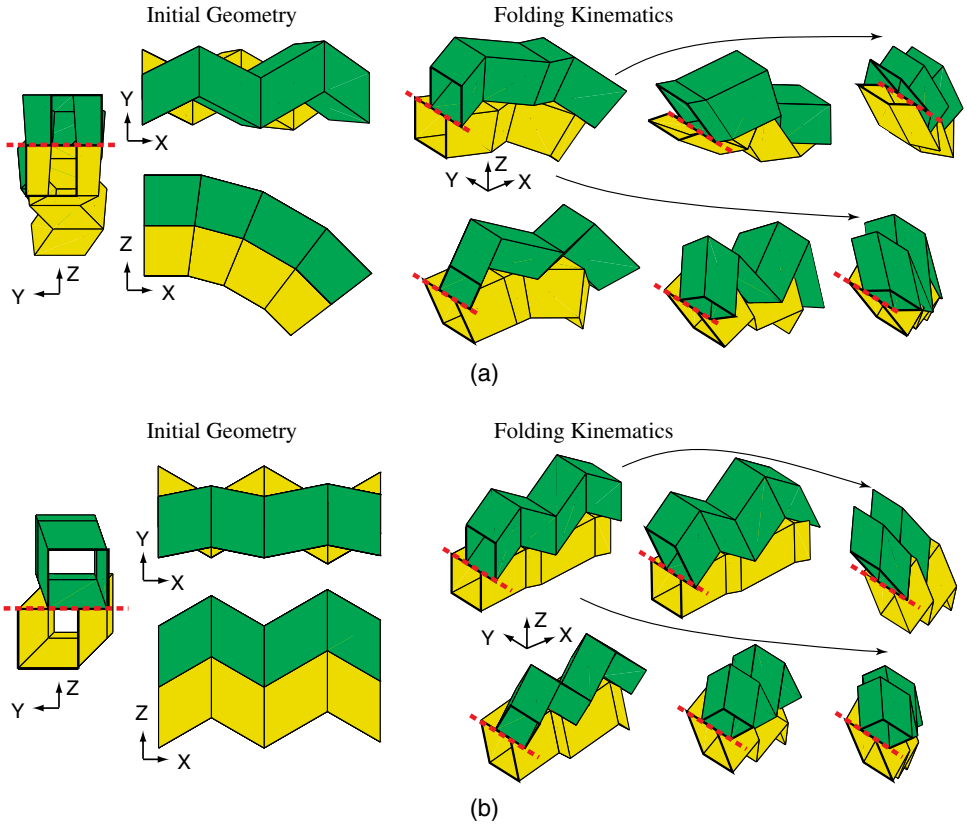

Fig. 6. Initial geometries and folding kinematics of two zipper-coupled tubes. A thick dotted line parallel to the Y-axis is shown as a reference for all configurations: (a) nonstraight tube with $\phi_{YT} = -\phi_{YB} = 30°$, $\phi_Z = 0°$, $\theta_T = \theta_B = 0°$, and $\epsilon_2 = \epsilon_3 = \epsilon_i = 7.5°$. Because $\phi_Z < \phi_Y$ the top and bottom folds can switch, leading to two different folding motions [similar to Fig. 5(b)]; and (b) straight zipper tube with $\phi_{YT} = 10°$, $\phi_{YB} = -30°$, $\phi_Z = 30°$, and $\theta_T = \theta_B = 0°$. The side folds of the top tube switch, leading to two different folding motions [similar to Fig. 5(c)]. The length of the projections for both zipper tubes is not constant: $l_1 = l_2 = l_4 = 1$ and $l_3 = 1.2$.

J. Struct. Eng., 2019, 145(2): 04018244

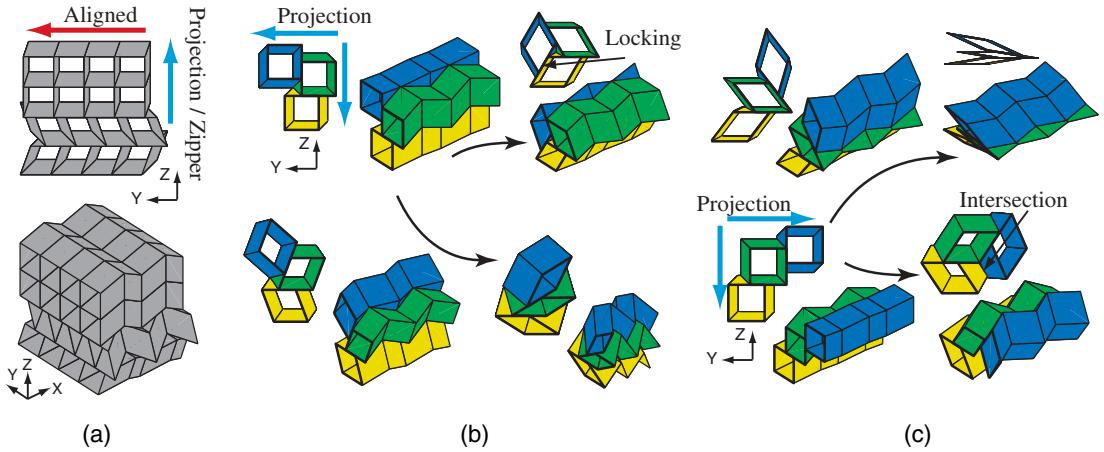

Fig. 7. Basic coupling arrangements for multiple origami tubes: (a) projection-based coupling of tubes with different cross sections in the Z-direction and aligned coupling Y-direction; and (b and c) projection-based coupling in two directions limits the system kinematics.

be continued effectively in one direction [Fig. 7(a)]. Using the projection-based technique in multiple directions leads to systems with self-locking and interactions that limit the folding motions [Figs. 7(b and c)]. An alternative is to use an aligned or repetitive coupling in which the same tube geometry and projection properties create an identical tube that conveniently has the same kinematic properties. The aligned coupling can also be used in multiple directions; in Fig. 7(a) the same tubes are repeated in the Y-direction, and the top two rows of tubes are identical.

It is possible to couple a larger variety of straight tubes, because the cross section can be changed when using the projection-based approach. For example, the parapets of the bridge type structure in Fig. 8(b) were created using a different geometry from the deck of the bridge. Curved systems that use projection coupling, however, must follow the limitation of symmetry as imposed previously (i.e., $\phi_{YT} = -\phi_{YB}$ and $\theta_T = -\theta_B$ or $\phi_{YT} = \phi_{YB}$ and $\theta_T = \theta_B$).

Using projection and aligned coupling simultaneously was of primary interest in this work, because the repetition would allow for the creation of large practical surfaces, including slabs, decks, hulls, canopies, and others. Once the projection-based technique is used to create two or more coupled tubes in the Z-direction, repetition is used to extend the system in the Y-direction. A benefit of aligned coupling in the Y-direction is that the global system becomes much like a membrane with a high global in-plane stiffness. The large surface can be used for diaphragm action that can transfer lateral loads between structural elements and act as a structural member. Another benefit of coupling in two directions is the creation of a cellular sandwich structure that can distribute forces

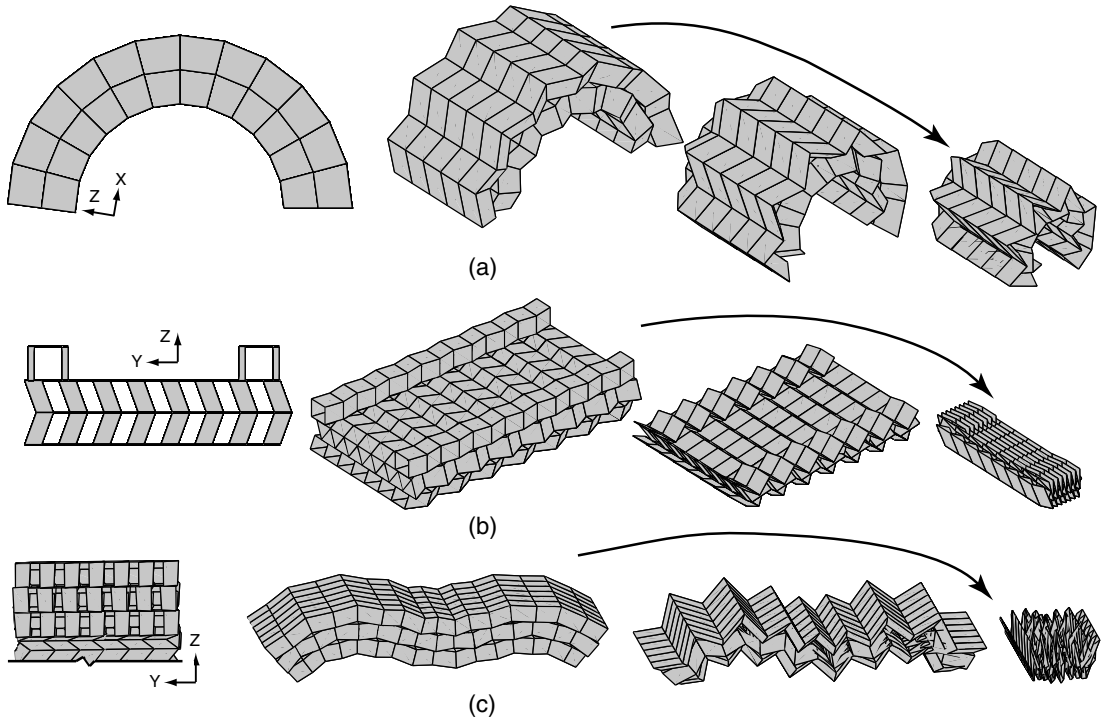

Fig. 8. Examples of smooth sandwich systems created by coupling multiple tubes: (a) arched vault; (b) bridge deck consisting of tubes with different cross sections; and (c) undulated canopy.

and stresses to multiple locations. The cellular nature also prevents local buckling and enhances the global stiffness of the structure. The subsequent sections will discuss the stiffness properties associated with the geometric design and show how to create stiff practical systems in which the top surfaces can be flat, similar to those shown in Fig. 8.

Analytical Procedure and Global Stiffness Characteristics

This work used a bar and hinge model to investigate the global structural characteristics of coupled origami tubes [specifically, the N5B8 model in Filipov et al. (2017)]. Although the bar and hinge approach cannot capture local behaviors of the origami, it is well suited for comparative and parametric studies of rigid foldable origami with quadrilateral panels such as the tubes explored in this paper. The model captures three distinct behaviors, including shear and stretching of the thin origami sheets, bending of the sheets, and folding along prescribed crease lines. The model is scalable with respect to thickness and length parameters, and it simulates geometric properties reasonably well (e.g., panel skew). For a detailed discussion of the model, its capabilities, and its formulation, the reader is referred to Filipov et al. (2017) and Filipov (2016).

For the deployable tubes in this work, we used arbitrary dimensions and material properties that were within a realistic range for origami. Whenever possible, unit dimensions (1) were used; for example, the cross sections and segment lengths of projections are 1 unless otherwise noted. The thickness of the material was defined as $t = 0.01$ such that the length to thickness ratio was generally $L{:}t \approx 100$. The fold line stiffness was defined with a length scale parameter of $L^* = 80$ mm which resulted in a fold to panel stiffness ratio of about $K_F{:}K_B \approx 1/5$. The actual local stiffness of a fold is found from $K_\ell = (L_F/L^*) * Et^3/(12(1-\nu^2))$, where L_F is the length of the fold [see Filipov et al. (2017) for details]. We used an arbitrary elastic modulus of $E = 10^6$ and a Poisson's ratio of $\nu = 1/3$. The units of the elastic modulus were in force per length squared, and stiffness for the different origami components (folds and panel) were appropriately calculated (Filipov et al. 2017). Although a specific unit basis was not selected for this work, any appropriate basis could be substituted (e.g., newtons and meters). The use of these arbitrary parameters was sufficient to allow for qualitative evaluation of behaviors and a comparative study between different origami geometries.

Our work used a small displacement formulation for the structural analysis and was primarily focused on comparing the stiffness of different origami geometries and system configurations. This analysis was well suited for capturing the initial stiffness of structures but not the stiffness if large displacements were experienced by the system. We envision that in their practical implementation, such deployable structures would be able to undergo large kinematic motions; however, the global stiffness should be high enough to prevent large structural displacements from applied loads. Designers would be able to use the geometry (e.g., number of tubes, depth, thickness, and so forth), and the material properties (elastic modulus and density) to improve the stiffness-to-weight behavior of the system. Their designs would ensure that for the given loads, the displacements would remain small enough (e.g., Δ/L over 2%) to ensure serviceability and prevent P-delta effects. The zipper-coupled systems explored here exhibited a desired behavior in which their deployment was flexible (achieved by the bending of flexible fold lines), yet they were substantially stiffer for other types of system deformation (behaviors independent from the flexible fold lines). The intrinsic properties were first explored in Filipov et al. (2015) and are briefly discussed in the following several paragraphs. Later in this work, we show simple physical models of stiff coupled tubes that can support much more than their self-weight while keeping displacements reasonably low ($\Delta/L \leq 2\%$). Our small-displacement analysis would likely estimate the deformed shape and stiffness of such cases well, but might significantly underestimate or overestimate the stiffness of more flexible structures that undergo large displacements from their applied loads.

Eigenvalue Analysis of Coupled Tube Systems

Studying the eigenvalues of an origami structure is a useful way to understand and characterize global stiffness properties. We obtain the eigenvalues (λ_i) from the linear elastic system of equations $\mathbf{K}v_i = \lambda_i \mathbf{M}v_i$, where $\mathbf{K}$ is the stiffness matrix, and $\mathbf{M}$ is the mass matrix of the structure (assuming an arbitrary density of $\rho = 1$ for the thin sheets). The eigenmode v_i represents a deformation mode and the corresponding eigenvalue is a representative stiffness for that deformation. In this analysis, no restraints were used, and thus the first six eigenmodes correspond to rigid body motions of the entire structure. The seventh eigenmode represents the kinematic folding motion of the origami, and subsequent eigenmodes represent structural deformations.

Fig. 9 shows the eigenvalues of a curved origami coupled tube for the entire folding sequence, which involves (1) an extension to full deployment (Configuration I); (2) a switching reconfiguration at a full deployment length of 3.81; and (3) another extension through which the system can retract (Configuration II). An important concept from this plot is that there is a large separation or band-gap between the seventh and eighth eigenvalues (note the logarithmic scale). The large band-gap is unique to the zipper type of coupling and represents the large difference in stiffness between the kinematic folding and other structural deformations. Other types of coupling such as aligned coupling (shown in the following section) also exhibit a band-gap but one that is not quite as significant (Filipov et al. 2015). Although the eigenvalues can represent the global system properties, they do not present an effective comparison for the different origami configurations or how the system would perform for practical applications. For example, although the eigenvalues change somewhat for the two folding paths, their connection to structural stiffness and practical implementation is not evident.

Static Analysis of Coupled Tube Systems

Static analyses are well suited to providing insight on practical applications and are useful for performing comparative studies on different origami geometries. To evaluate the bending stiffness of the coupled tube structures, we perform a three-point bending test on tubes with ten segments in the X-direction. The tubes are closed off on both ends with thin sheet panels to restrict the global folding motion. The system is vertically supported on both ends, but it is free to expand lengthwise and orthogonally. A perpendicular unit load is applied at the middle of the tube in the Z-direction and is distributed to the nodes at that plane such that the total load is $F_Z = 1$. A representative stiffness of the structure for the Z-direction is then calculated as $K_Z = F_Z/\Delta_Z = 1/\Delta_Z$, based on the average displacement of the loaded nodes Δ_Z. For completeness, in this section we also evaluate the stiffness in the Y-direction (K_Y). However, the Y-direction stiffness is assumed less important because most applications will use aligned coupling in the

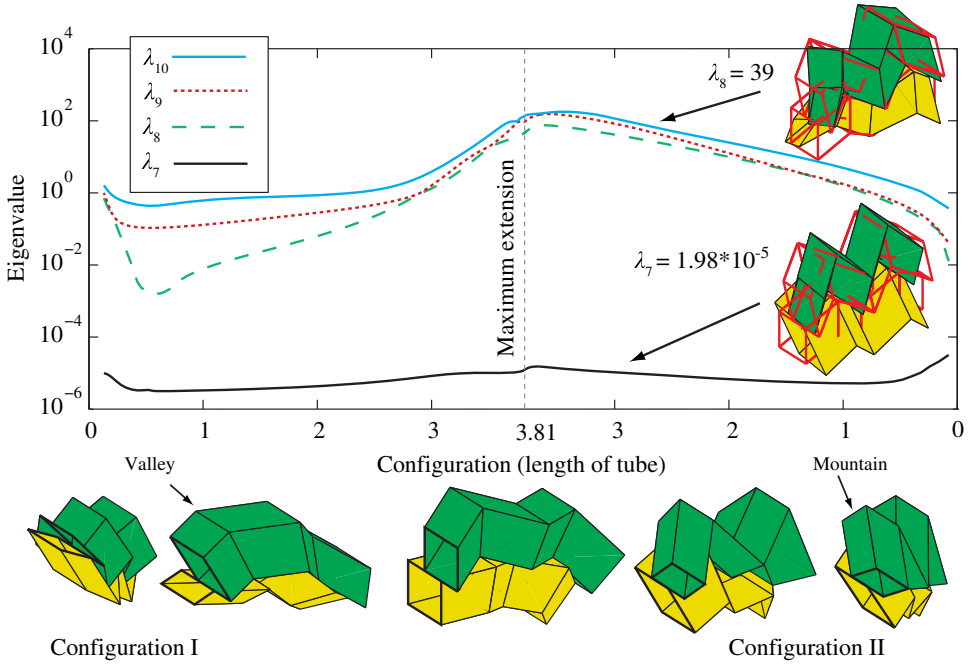

Fig. 9. Eigenvalues of coupled curved tube with respect to the length of the system (measured at the coupling surface on the two farthest ends). An increasing and decreasing horizontal axis represents the two distinct configurations of the tube structure. A large eigenvalue band-gap ($\beta = \lambda_8 - \lambda_7$) is present in all configurations.

Y-direction, thereby greatly enhancing the total in-plane structural stiffness.

Fig. 10 shows static analysis for three coupled tube beams with different geometric properties. The first system corresponds to a classic zipper-coupled tube (Filipov et al. 2015), in which both tubes are partially developable and have equal and opposite Y-projections. The second case is an intermediate case in which the top tube is partially developable, but the bottom tube has a shallower Y-projection ($\phi_Y = -10°$). The last case is an aligned coupled case of two identical tubes. The deformed shapes for the zipper and intermediate tubes are generally uniform, with the beam deforming with near constant curvature and little local deformation. The aligned tube system, however, has a varied deformation over its length, with local deformations occurring. The tube expands substantially (deforms in the X-direction) despite the fact that the two ends of the tube are restricted from folding. The side and top geometries changed from the support to the middle of the beam, indicating local deformations and a squeezing type of motion in which only portions of the structure fold. The aligned tubes have a smaller eigenvalue band-gap and are more prone to these types of squeezing deformations.

In Fig. 10 the deformed shapes are scaled such that the maximum displacement is equal and cannot be used to compare stiffness. Instead, the vertical (K_Z) and horizontal (K_Y) stiffness are shown in Figs. 10(d and e), respectively, for different configurations. The configuration of the tube is presented as the length of the tube. When the aligned and zipper tube extend fully, they lay flat in the X, Y-plane, reaching the maximum length of the flattened coupling surface (10 units). However, the intermediate tube can only reach a length of 8.9, at which point the side folds of the bottom tube switch, and the structure retracts. The switching leads the system to have two separate curves for stiffness, each corresponding to one of the folding sequences (Configuration I or II). In most scenarios, the classic zipper-coupled tubes have a higher stiffness than the other two cases, except around the maximum extension of the intermediate tube. At that point, the lower tube ($\phi_Y = -10°$) has a square cross section and is able to brace the structure in both directions. The intermediate tube has a stiffer and more flexible branch, which is typical for many of the reconfigurable coupled tubes. In scenarios with reconfiguration, we focus primarily on the stiffer of the two branches.

In the following sections, we look at more generally comparing the stiffness of coupled tubes with different geometries. Thus, we use points of interest on the stiffness curves that correspond to different deployment configurations. For the vertical stiffness analyses, we obtain the points K_{Z2}, K_{Z5}, K_{Z8}, and K_{ZMAX}, representing the stiffness at configuration lengths of 2, 5, 8, and the peak (maximum) vertical stiffness at any configuration. Fig. 10(e) shows that in some configurations the maximum stiffness may provide misleading results. At a configuration length of 10, both the aligned and zipper tubes have a maximum horizontal stiffness (K_{YMAX}); however, in this configuration the systems are completely flat in the X, Y-plane and have no stiffness in the Z-direction, so they may not be practically useful. Similarly, it is also important to consider the full extension sequence and possibly different branches. Although the intermediate tube has the highest K_{ZMAX}, its vertical stiffness is about one fourth of the stiffness of the zipper tubes when at a configuration length of 2 in the Configuration II folding sequence.

Bending Modulus of the Tubes

The static analyses can be further postprocessed to calculate a representative bending modulus for the different coupled tube beam structures. Assuming the system will deform as a uniform, slender, simply supported beam with a load applied at the midspan, the bending modulus can be back-calculated as $I_B = F_Z * L^3/(48E\Delta_Z)$. The length of the beam is L and the maximum

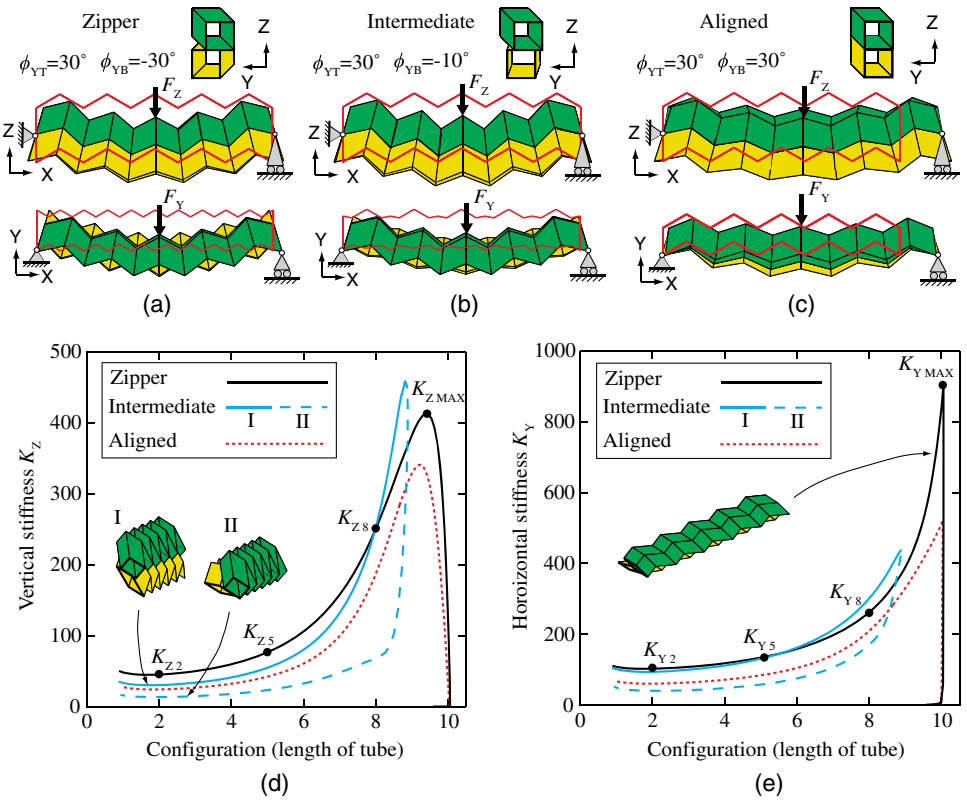

Fig. 10. Static analysis of origami tubes. Tubes are subjected to a three-point bending test in which the ends are restrained from folding and a load is applied in the middle of the beam. Initial (outline only) and deformed geometry for Y- and Z-direction tests of the (a) zipper ($\phi_{YT} = -\phi_{YB} = 30°$); (b) intermediate ($\phi_{YT} = 30°$, $\phi_{YB} = -10°$); (c) aligned ($\phi_{YT} = \phi_{YB} = 30°$) tubes. The deformed shapes are scaled so that the maximum displacement is equal to the cross section width (=1) and do not necessarily represent stiffness; (d) stiffness in the vertical direction (K_Z) versus folding configuration (length of structure). The intermediate tube has a different stiffness for the two folding directions (I versus II); and (e) stiffness in the horizontal direction (K_Y) versus folding configuration (length of structure). Stiffness values of interest for the zipper tube are indicated (e.g., K_{Y5} horizontal stiffness at length 5).

vertical displacement (Δ_Z) is assumed to occur at the midspan. Fig. 11 shows the bending modulus of the zipper, intermediate, and aligned tube structures with respect to the number of segments in the beam. The systems are all at the same extended state, corresponding to a configuration length of 8 for the 10-segment tube (e.g., an extended length of 4.8 for a 6-segment tube or 16 for a 20-segment tube). As the number of segments in the systems increase, the bending modulus increases and converges, because a more pure bending occurs over the length of the system and local shear deformations are reduced. Practical designers may thus consider using longer and more slender tubular systems with more segments in order to harness the higher modulus and limit the shear deformations. However, this would require stacking more tubes in the Z-direction to achieve the desired total stiffness. Similar to the results shown before, the zipper-coupled tube has a higher stiffness and thus a higher bending modulus than the other tubes cases. The lower stiffness in the aligned tube can be attributed to the squeezing deformation motion, which also leads to the tube expanding in the X-direction. Because the calculated stiffness (e.g., K_{Z8}) and bending modulus for different systems tend to correspond well, we limit the remainder of the analyses in this paper to calculating only the representative stiffness. However, the results of bending moduli for different systems could be useful for future practical design. During preliminary design, a user may want to choose the length and bending modulus to optimize for material usage and stiffness.

Deployable Tubes with Flat (Smooth) Surfaces

With the aim of tailoring these systems for practical applications, we explore the vertical stiffness of two coupled tubes (a beam system) that can achieve a flat surface on top when fully deployed. This geometry is useful for creating deployable slabs, decks, walls, and other smooth structures. In addition to their functionality, the deployable systems may be more aesthetically pleasing than the segmented systems currently available.

First, we explore the change in vertical stiffness when the cross section transitions from a conventional zipper tube to a system with a flattened top. Fig. 12 presents two cases in which a conventional zipper tube is used as a base ($\phi_Z = \phi_{YT} = -\phi_{YB} = 30°$) and is varied using parameter ϕ_{VAR} in order to reach a system with a flat top. In Case 1 ($\phi_{VAR} = \phi_Z = \phi_{YT} = -\phi_{YB}$), all projections are varied together, and the systems are always partially developable; in Case 2 ($\phi_{VAR} = \phi_Z$), only the Z-projection of the coupling surface is varied, and the Y-projections remain constant. The two cases both approach a case of having a flattened top when ϕ_{VAR} approaches zero.

The vertical stiffness with respect to the parameter ϕ_{VAR} is presented in Fig. 12(b). For clarity, only the folding path that provides higher stiffness is shown (e.g., the maximum K_{Z5} from the folding paths I and II). The results show that the maximum vertical stiffness (K_{ZMAX}) can typically be increased by making the tubes more square and less zigzagged (by reducing ϕ_{VAR}). However, as

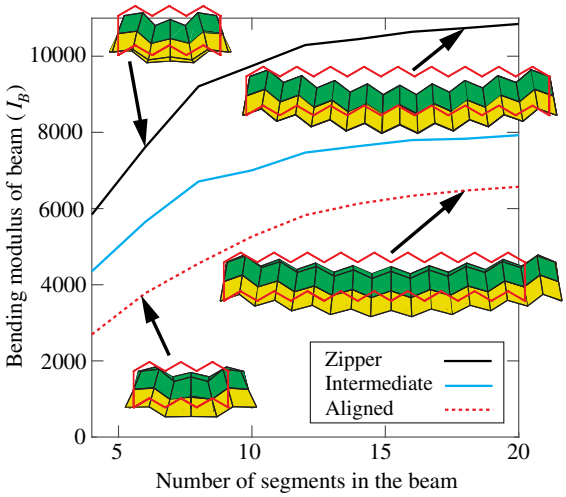

Fig. 11. Bending modulus of the zipper, intermediate, and aligned tube systems versus the number of segments in the beam. Representative deformed geometries are shown for the zipper and aligned cases with 6 and 18 segments. The deformed shapes are scaled so that the maximum displacement is equal to the cross section width (=1) and do not necessarily represent stiffness.

ϕ_{VAR} approaches zero, the vertical stiffness during deployment configurations (at lengths of 2, 5, and 8) decreases significantly. Thus, the conventional zipper tube has high stiffness during deployment, but flattening the tube for practical applications reduces this stiffness significantly. Case 2, in which the Y-projection is maintained, has a higher stiffness during deployment than the partially developable tubes; however, it is substantially less stiff than the conventional zipper.

To address the decrease in stiffness from the flattening of the tube, we next explore how changing the cross sections of the tubes can be used to tailor the stiffness properties to create a system with reasonably high vertical (Z-direction) stiffness during deployment. Straight tubes are defined with a Z-projection of $\phi_Z = 0°$ such that they have a flat top surface, and with ten segment lengths of $l_1 = l_2 = l_i = 1$. The tubes are defined such that in their initial configuration they are fully deployed, have a flat top surface, and have a total span of 10. Because the tubes are straight, it is possible to have nonsymmetric top and bottom tube projections and cross sections. Fig. 12 shows that increasing the ϕ_Y projections can increase the stiffness during deployment; for this reason, here we explore only the influence of cross section variations. The Y-projections are kept the same ($\phi_{YT} = -\phi_{YB} = 30°$), and the cross section angles are now varied with the parameter θ_{VAR}.

Fig. 13 presents three cross section variations: Case 1 ($\theta_{VAR} = -\theta_B$), in which only the bottom tube cross section is varied; Case 2 ($\theta_{VAR} = \theta_T = \theta_B$), in which the top and bottom cross sections are rotated in the same direction; and Case 3 ($\theta_{VAR} = \theta_T = -\theta_B$), in which the top and bottom cross sections are rotated in opposite directions (i.e., appear mirrored about the Y, X-plane). All cross section variations reduce the peak vertical stiffness (K_{ZMAX}) of the system, but they increase the stiffness during deployment. In particular, Case 3 substantially increases the vertical stiffness in intermediate deployment configurations. Case 3, in which the tube cross sections are rotated in opposite directions, provides the best design alternative for slab-type systems in which a flat surface and a reasonable vertical stiffness are needed simultaneously. This system would provide a high orthogonal stiffness during deployment and would not substantially reduce the peak vertical stiffness. The structures would be well suited for application in practice, as this geometry would require the least material in order for the self-weight to be effectively supported during deployment.

Influence of Tube Geometry on Vertical Stiffness

To explore the influence of reconfiguration and cross section geometry on stiffness at various points of deployment, Fig. 14 compares three tubes with different Z-projections and cross section geometries (all tubes have the same Y-projection, $\phi_{YT} = -\phi_{YB} = 30°$). The first tube is a *zipper* tube identical to the tube presented in Fig. 10(a) ($\phi_Z = 30°$). The second tube has a *flat* top and square cross sections ($\phi_Z = 0°$). The last tube has a flat top and a *skewed* cross section ($\theta_T = -\theta_B = -30°$).

The kinematic motions of the three tube cases presented in Fig. 14 are different. The *zipper*-coupled tube does not reconfigure and follows one continuous motion from a folded system in the Y, Z-plane to a flattened system in the X, Y-plane. Over most of the motion, the zipper tube has a wide and deep profile (i.e., section view in the X, Z-plane). Due to this cross section, the structure typically has higher vertical stiffness when compared with the other two structures.

The *flat* system with a square cross section is initially defined at a fully deployed state. When fully deployed, it has the highest vertical stiffness, because the side panels are orthogonal to the

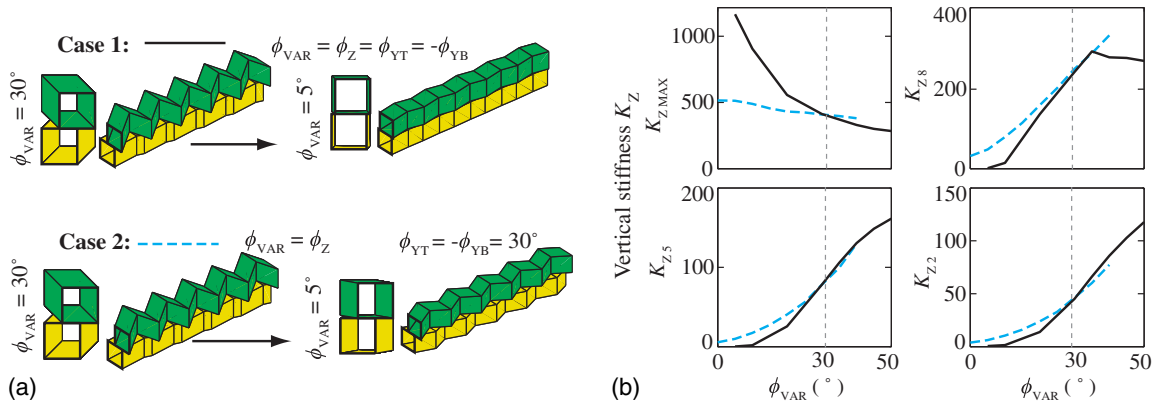

Fig. 12. (a) Two variation cases in which the projection angles are varied to create a system with a flat top surface; and (b) vertical stiffness with respect to the variation of projection for the two cases. The peak K_{ZMAX} and stiffness at different configurations are shown (e.g., K_{Z5} stiffness at length 5).

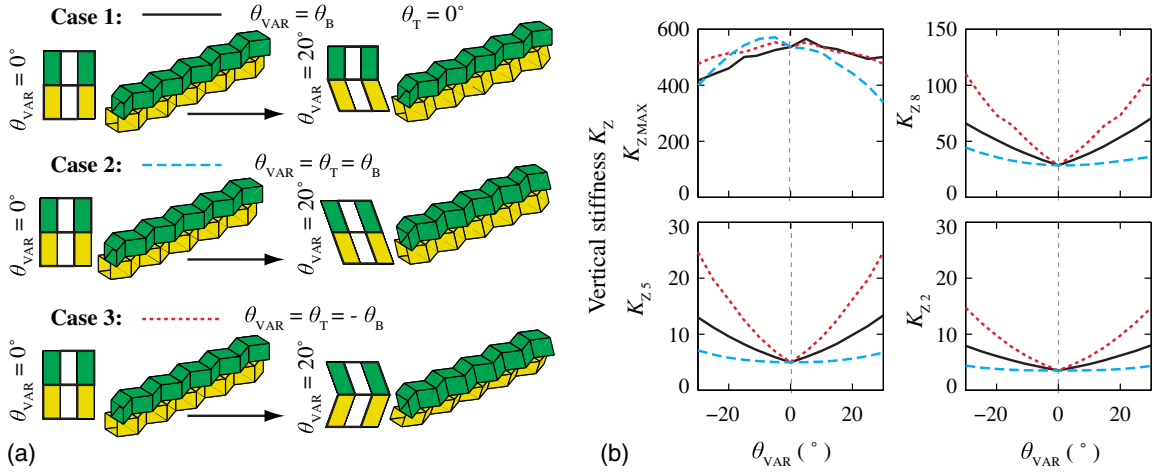

Fig. 13. Influence of cross section geometry on stiffness for coupled tubes in which the top surface is flat ($\phi_Z = 0°$): (a) three cases that depict variations of the cross section angles; and (b) vertical stiffness with respect to cross section variations presented as the peak stiffness K_{ZMAX} and at different points of deployment (e.g., K_{Z5} vertical stiffness at length 5). Case 3, in which the cross section is mirrored about the Y-axis, presents a significant increase in stiffness during the deployment sequence.

applied load. The structure can retract in two symmetric motions. The vertical stiffness for these two motions is the same (the plots for motions I and II overlap), and the stiffness is close to zero when the system approaches a stowed configuration (length <6). The profile (in $X - Z$) of the tube is more shallow than the zipper, and it approaches a triangular, accordionlike shape when stowed.

The *skewed* cross section system has two different reconfiguration motions. Motion I has a deeper profile (in $X - Z$) and a higher stiffness in the vertical direction. The profile through motion I deployment is deeper and wider than the flat tube with a square cross section; however, it is shallower than the zipper tube in the same configurations. Motion II has a narrow profile in $X - Z$ and low out-of-plane stiffness.

The vertical depth of the tube and the internal volume of the system relate to the stiffness properties. Fig. 14(b) shows that deeper profiles in the Z-direction and a larger internal volume (during deployment) lead to higher stiffness, although these do not correlate linearly. The behavior can be explained by looking at the system as a three-dimensional beam for which a deeper section leads to a higher bending modulus. The deployable structures are stiffest when they are close to fully deployed. At deployed configurations their cross sections are open and they behave like deep beams. When retracting, all tubes become more flexible because their profile approaches more of a triangular wave and accordion-like shape. Narrow profiles and triangular geometry lead to lower bending stiffness. Finally, it should be noted that the skewed tube has one reconfigurable motion of higher out-of-plane stiffness.

Verification of Stiffness Characteristics

In Fig. 15, physical models of the flat and skewed coupled tubes are used to demonstrate the concepts of stiffness properties at different points of deployment. The models were created with paper card stock with a weight of 160 g/m^2 and approximate thickness of 0.25 mm. The folds were created by fully perforating the material with cuts of 0.5 mm spaced evenly every 1 mm. To achieve a length to thickness ratio of $L{:}t \approx 100$, the cross section dimensions and projection lengths were all set to 25 mm. For simplicity, one unit (panel dimension) is equal to 25 mm and the extension (ex) is classified based on the number of units; for example, an extension of $ex = 10$ is a fully extended system, while a system with $ex = 8$ is a structure folded to a span of 200 mm. These unit extensions correspond to the configuration of the tubes presented previously in Fig. 14. Models were constructed of the flat and skewed variations to show the difference in stiffness that each system has. Each of the coupled tube structures weighed around 10 g, but both could carry loads that were much greater than their self-weight. The models were loaded with steel weights, and displacements at the midpoint of the structures (Δ) were measured from photographs before and after loading. The camera was placed 50 cm directly in front of the beams, and a ruler was placed behind the samples to visually approximate the displacements in the photographs. Fig. 15 shows that, when fully extended, both systems carried a 500 g weight with little deflection ($\Delta = 1$ mm for the flat and $\Delta = 2$ mm for the skewed). The deformations in the skewed system were primarily localized at the supports. When retracted, the flat system became more flexible and experienced large deflections when loaded with 200-g ($\Delta = 16$ mm) and 100-g ($\Delta = 19$ mm) weights at extensions of $ex = 8$ and $ex = 5$, respectively. The skewed system retained reasonable stiffness at these configurations and carried a 200-g weight without a substantial deflection ($\Delta = 4$ mm at $ex = 8$ and $\Delta = 3$ mm at $ex = 5$). Only the stiff motion (I) branch is shown for the skewed tube; the flexible branch experienced a large deflection when retracted and loaded with a smaller weight (100 g). The experiments presented in Fig. 15 serve only to demonstrate the concept that the coupled tube systems can carry more than their self-weight during deployment. They can support large loads (e.g., 20× self-weight) while effectively keeping displacements relatively low (e.g., $\Delta/L = 4/200 = 2\%$). A rigorous experimental program with multiple samples should be performed to quantitatively verify and evaluate the stiffness properties of these and related systems.

The parametric study in Fig. 16 shows the influence of the elastic modulus E, the thickness t, and the fold length scale parameter L^* on the stiffness. The skewed structure with ten segment lengths, a flat top, and a cross section of $\theta_T = -\theta_B = -30°$[the same cross section as in Fig. 14(e)] is evaluated by changing each parameter separately. Both the maximum stiffness and the stiffness at a deployed length of 5 scale linearly with E. This scaling is to be expected, because the stiffness of all components of the origami scale directly with the elastic modulus. Stiffness also scales approximately linearly with the thickness t. This scaling shows that the

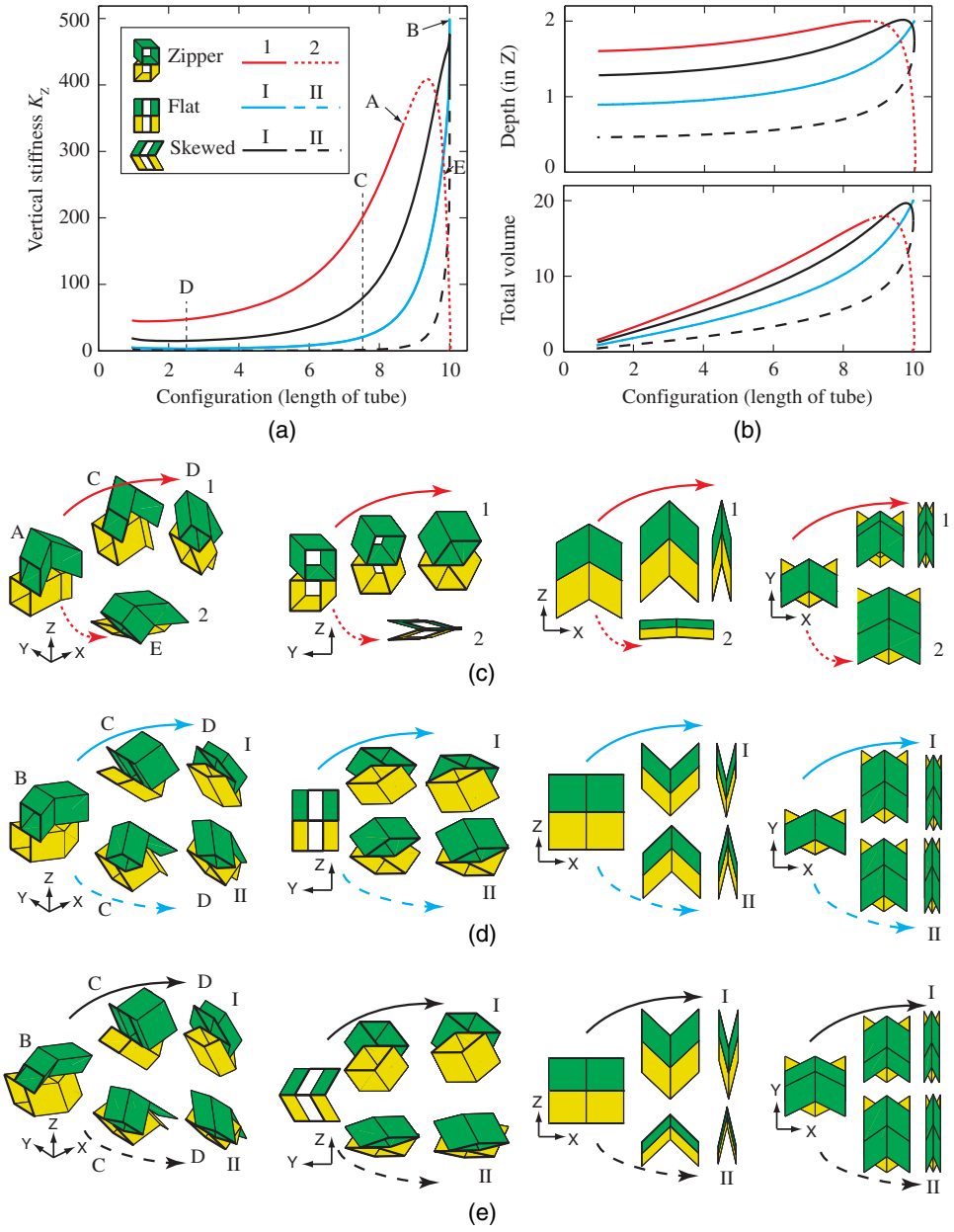

Fig. 14. Influence of profile geometry on stiffness: (a) vertical stiffness of the zipper, flat, and skewed tubes with ten segment lengths. Solid and dotted lines show the kinematic motion starting from the initial state; (b) tube depth and volume with respect to configuration. Isometric and section views depict the motion of unit cells of (c) zipper; (d) flat; and (e) skewed tubes. The views are shown at initial configurations (A and B), as well as 7.5 (C), 2.5 (D), and 9.9 (E) deployment.

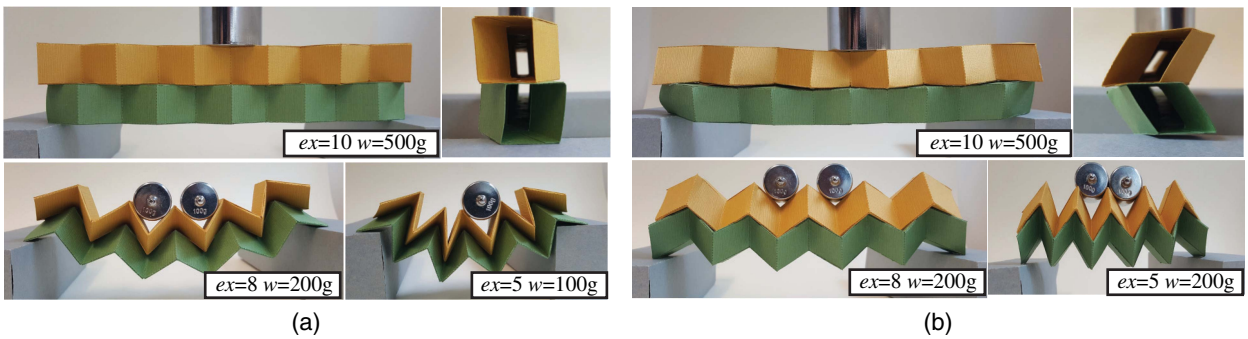

Fig. 15. Physical verification: (a) flat tube system with initially square cross section; and (b) the flat system with a skewed cross section. The tubes, loaded in different configurations, are shown at approximate extension *ex* in terms of number of segments and the applied weight *w*.

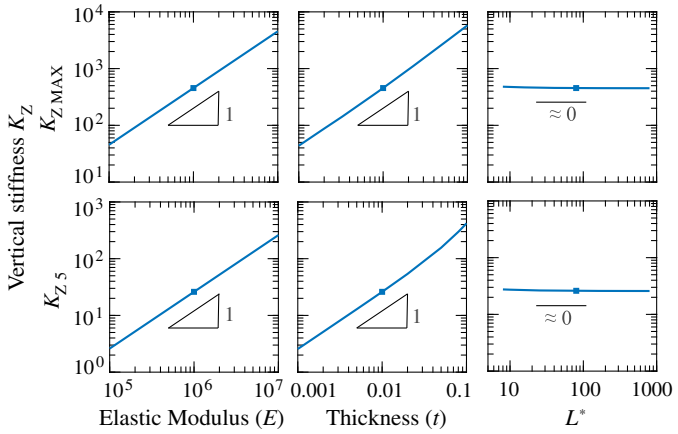

Fig. 16. Influence of model parameters on the peak vertical stiffness K_{ZMAX} and the stiffness at a deployment length of 5 (K_{Z5}). Stiffness scales linearly with the elastic modulus and thickness, and it is not significantly affected by the fold line length scale L^*. The square marker corresponds to the initial skewed structure in Fig. 14.

stiffness is directly related to the stretching and shearing of the panels (whose stiffness scales with t) and not to the bending of panels or fold lines (both of which scale with t^3). Increasing the length scale parameter L^* (thereby decreasing the fold stiffness) only slightly decreases the overall stiffness of the structure and has a negligible effect when compared to other parameters. This observation further verifies that stretching and shearing are the primary means of carrying loads in this skewed variation of zipper tube structures. Carrying loads through stretching and shearing is more efficient than bending and allows for a global moment to be generated over the depth of the system. The parametric study further shows that the stiffness could be increased by modifying the material properties (E) and thickness (t). We expect that a physical demonstration would scale appropriately with other materials and would allow for practical structures that can carry more than their self-weight. However, when attempting practical extensions, we recommend that detailed analytical studies be performed to ensure that the displacements remain reasonably low (e.g., within 1%–2%). For example, we do not believe that our analysis effectively represents the deformed state and stiffness of the flat prototype shown at the bottom of Fig. 15(a). Prior to practical implementation, systematic experiments should be performed to investigate how material properties and fold characteristics influence the performance of such structures.

Structural Systems with Rise

In this section, we investigate the stiffness of different simply supported geometries that can span a distance and also provide a rise and clearance. First, three roof shapes are compared, and the influence of increasing rise on total stiffness is explored. A gable, a barn (gambrel), and curve-shaped roofs are created with an initially flat top (Z-projection of $\phi_Z = 0°$) and with skewed cross sections ($\theta_T = -\theta_B = -30°$). The tubes have twelve segments with a constant segment length of $l_1 = l_2 = l_i = 1$. The gable roof is constructed with two straight tube sections and with one cross section rotation in the middle of the span ($\epsilon_7 \neq 0$). By increasing the cross section plane rotation, the rise increases and the span of the structure decreases. The barn (gambrel) roof consists of four straight tube sections, with three equivalent plane rotations ($\epsilon_4 = \epsilon_7 = \epsilon_{10} \neq 0$). The curved shape is defined with the projection plane rotated equivalently over the length with $\epsilon_2 = \epsilon_3 = \epsilon_i$. Schematics and the span versus rise relations for the three structures are shown in Fig. 17.

A three-point bending test similar to that done in previous sections is used to explore the stiffness of the simply supported structures with rise. The analysis is linear elastic, and small deformations of the structures are considered. Fig. 18 shows the vertical stiffness of the roof structures with respect to their deployment. Because all the structures have different dimensions, we show intermediate stiffness with respect to the maximum span dimension; for example, $K_{Z1/4s}$ corresponds to the vertical stiffness when the deployment is at quarter span.

To allow for a straightforward comparison with previous sections, the systems with a rise of $r = 0$ correspond to straight tubes. As the rise of the barn and the curved systems increases, they have a higher maximum vertical stiffness K_{ZMAX}. This increase is likely because the curved geometry better distributes the in-plane loads from the load to the support. Curved geometries are well known to be efficient at carrying vertical loads between two supports [e.g., Tyas et al. (2011)]. When loaded at a fully deployed state, the structures experience a spread with the two ends moving apart [Fig. 18(a)]. The gable has a lower peak stiffness for a rise higher than about 1; this may be due to the observed spreading behavior.

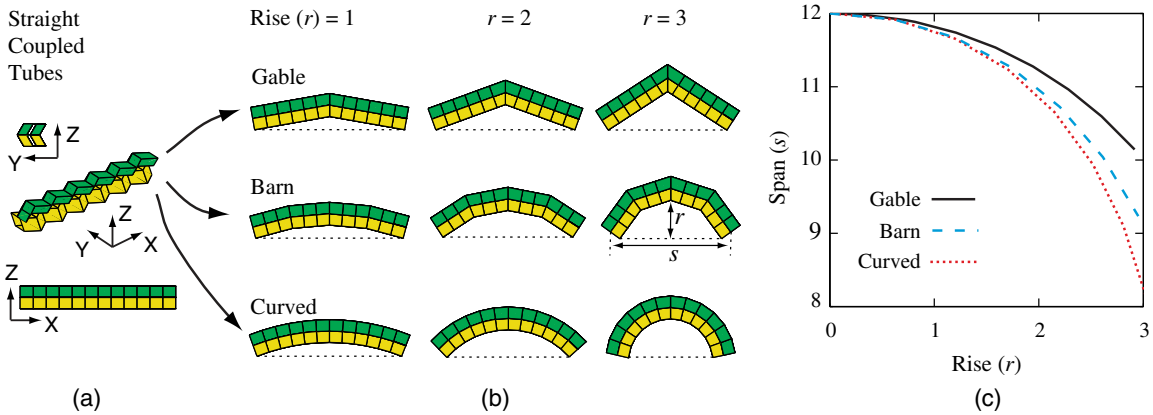

Fig. 17. Geometry of different deployable roof structures: (a) straight flat tube with a skewed cross section that is used as an initial basis for the modified roofs; (b) gable, barn (gambrel), and curved roof structures shown with increasing rise r from left to right; and (c) rise versus span for the different structures. The length of the coupling surface is the same for all geometries and this leads to the different rise to span relations.

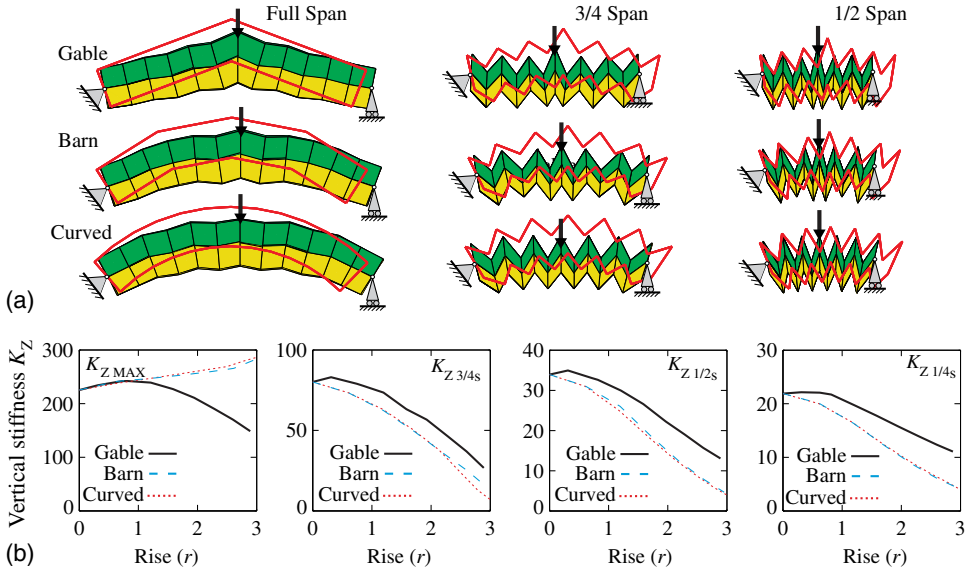

Fig. 18. Static, linear elastic analysis of the gable, barn (gambrel), and curved roofs: (a) deformed shapes for the three roofs with a rise of two (2) shown at different configurations. Initial shape is shown with an outline, and deformed shapes are scaled so that the maximum displacements are equal to one twelfth of the span ($s/12$) and do not necessarily represent stiffness; and (b) vertical stiffness of the roof structures shown with respect to the rise r at different configurations.

All three roof systems have a peak stiffness near their full deployment, and the vertical stiffness is much lower in intermediate deployment stages (similar to the behavior of straight tube structures). In the intermediate deployment stages the vertical stiffness decreases with increased rise. The curved profiles lead to a more accordionlike shape during deployment. The gable roof tends to have a higher stiffness during deployment; this is likely because the cross section projection is only rotated at one point. In practice, the gable geometry presented here may pose problems, because high stress concentrations would develop at the apex of the gable. Changing the cross sections of these systems leads to results similar to those observed in straight tubes in which skewed sections lead to higher stiffness (Filipov 2016).

Concluding Remarks

This paper presents a generalized approach for creating coupled origami tubes by projecting quadrilateral cross sections in three dimensional space. The framework allows for the construction of both straight and curved tubes that can have segments of different lengths and cross sections. When tubes are coupled and stacked in multiple directions, it is possible to create flat and smooth deployable sandwich surfaces. The tube systems are created to be both rigid and flat foldable, meaning that they can fold into a compact two-dimensional state with kinematic motion facilitated by folding only along fold lines. Depending on the cross section and projection properties, the tubes could be partially developable, meaning that parts of them could be made by folding a single flat sheet. Some of the coupled tube systems could be reconfigurable, meaning that they can deploy and retract through two or more motions. The folding motions have different kinematics and result in different physical properties of the tubes.

The orthogonal stiffness of the coupled tubes was explored by performing three-point bending analyses and physical tests. Conventional zipper-coupled tubes have a higher bending stiffness than aligned tubes because squeezing motions are restrained. However, when modifying the zipper geometry to create structures with a flat surface, the design can result in systems with a lower orthogonal stiffness, especially at intermediate configurations during deployment. To improve the stiffness during deployment, it is possible to use skewed cross sections for the coupled tube structures. The skewed cross sections and more zigzagged projection geometries tend to create more open tube systems that have a higher bending modulus, which would be useful for practical structures. Physical prototypes of the skewed coupled tubes carried loads much larger than their self-weight with little observed deflection. The work also explored nonstraight structures that can create a rise, including the shapes of a gable, a barn (gambrel), and curved roof types. Increasing the rise (higher curvature) of these systems tends to increase the peak stiffness but reduces stiffness at intermediate deployment states. Based on the aforementioned motivation (e.g., see the introduction), the coupled tube sandwich systems presented in this work could lead to deployable structures where both high out-of-plane stiffness and geometric versatility (e.g., smooth curved surfaces) are required. However, there are still open research questions that need to be addressed to transition these structures into practical implementation. The cross-sectional width and height, length of segments, number of segments, number of stacked tubes, and thickness to length ratios could be optimized to improve the stiffness and functionality for specific design problems. Additionally, materials, fabrication methods, connections, supports, and actuation mechanisms all need further investigation when structures are conceived and designed for use in practice. This work provides a basis for these proposed future investigations.

Acknowledgments

The first author would like to acknowledge support from the University of Michigan and the National Science Foundation (NSF) GRFP and GROW fellowship grants. The authors also acknowledge support from NSF Grant No. CMMI 1538830, the Japan Science and Technology Agency Presto program, and the Raymond Allen Jones Chair at the Georgia Institute of Technology.

References

Ballard, Z. C., E. J. Gerbo, A. P. Thrall, and B. J. Smith. 2016. "Behavior of sandwich panels in a deployable structure." *J. Struct. Eng.* 142 (10): 04016073. https://doi.org/10.1061/(ASCE)ST.1943-541X.0001537.

Cai, J., X. Deng, Y. Xu, and J. Feng. 2015. "Geometry and motion analysis of origami-based deployable shelter structures." *J. Struct. Eng.* 141 (10): 06015001. https://doi.org/10.1061/(ASCE)ST.1943-541X.0001238.

Cheung, K. C., T. Tachi, S. Calisch, and K. Miura. 2014. "Origami interleaved tube cellular materials." *Smart Mater. Struct.* 23 (9): 094012. https://doi.org/10.1088/0964-1726/23/9/094012.

Del Grosso, A. E., and P. Basso. 2010. "Adaptive building skin structures." *Smart Mater. Struct.* 19 (12): 124011. https://doi.org/10.1088/0964-1726/19/12/124011.

Filipov, E. T. 2016. "Tailoring stiffness of deployable origami structures." Ph.D. thesis, Dept. of Civil and Environmental Engineering, Univ. of Illinois at Urbana–Champaign.

Filipov, E. T., K. Liu, T. Tachi, M. Schenk, and G. H. Paulino. 2017. "Bar and hinge models for scalable analysis of origami." *Int. J. Solid Struct.* 124: 26–45. https://doi.org/10.1016/j.ijsolstr.2017.05.028.

Filipov, E. T., T. Tachi, and G. H. Paulino. 2015. "Origami tubes assembled into stiff, yet reconfigurable structures and metamaterials." *Proc. Natl. Acad. Sci. U.S.A.* 112 (40): 12321–12326. https://doi.org/10.1073/pnas.1509465112.

Filipov, E. T., T. Tachi, and G. H. Paulino. 2016. "Origami tubes with reconfigurable polygonal cross-sections." *Proc. R. Soc. A* 472 (2185): 20150607. https://doi.org/10.1098/rspa.2015.0607.

Gattas, J. M., W. Lv, and Y. Chen. 2017. "Rigid-foldable tubular arches." *Eng. Struct.* 145: 246–253. https://doi.org/10.1016/j.engstruct.2017.04.037.

Gattas, J. M., W. Wu, and Z. You. 2013. "Miura-base rigid origami: Parameterizations of first-level derivative and piecewise geometries." *J. Mech. Des.* 135 (11): 111011. https://doi.org/10.1115/1.4025380.

Gattas, J. M., and Z. You. 2015. "Geometric assembly of rigid-foldable morphing sandwich structures." *Eng. Struct.* 94: 149–159. https://doi.org/10.1016/j.engstruct.2015.03.019.

Hull, T. C. 2012. *Project origami: Activities for exploring mathematics*. 2nd ed. Boca Raton, FL: CRC Press.

Lee, T. U., and J. M. Gattas. 2016. "Geometric design and construction of structurally stabilized accordion shelters." *J. Mech. Rob.* 8 (3): 031009. https://doi.org/10.1115/1.4032441.

Martinez-Martin, F. J., and A. P. Thrall. 2014. "Honeycomb core sandwich panels for origami-inspired deployable shelters: Multi-objective optimization for minimum weight and maximum energy efficiency." *Eng. Struct.* 69: 158–167. https://doi.org/10.1016/j.engstruct.2014.03.012.

Miura, K. 2009. "The science of Miura-ori: A review." In *Proc., 4th Int. Meeting of Origami Science, Mathematics, and Education*, edited by R. J. Lang, 8799. Natick, MA: AK Peters.

Miura, K., and T. Tachi. 2010. "Synthesis of rigid-foldable cylindrical polyhedra." In *Proc., Int. Society for the Interdisciplinary Study of Symmetry*, 204–313. Budapest, Hungary: International Society for the Interdisciplinary Study of Symmetry.

Morris, E., D. A. McAdams, and R. Malak. 2016. "The state of the art of origami-inspired products: A review." In *Proc., ASME IDETC/CIE Conf.* New York: American Society of Mechanical Engineering.

Randall, C. L., E. Gultepe, and D. H. Gracias. 2012. "Self-folding devices and materials for biomedical applications." *Trends Biotech.* 30 (3): 138–146. https://doi.org/10.1016/j.tibtech.2011.06.013.

Schenk, M., and S. D. Guest. 2013. "Geometry of Miura-folded metamaterials." *Proc. Natl. Acad. Sci. U.S.A.* 110 (9): 3276–3281. https://doi.org/10.1073/pnas.1217998110.

Tachi, T. 2009. "One-DOF cylindrical deployable structures with rigid quadrilateral panels." In *Proc., Int. Association Shell Spatial Structures*, 2295–2305. Madrid, Spain: International Association for Shell and Spatial Structures.

Tachi, T., E. T. Filipov, and G. H. Paulino. 2015. "Deployable folded-core sandwich panels guided by a generating surface." In *Proc., Int. Association Shell Spatial Structures*. Madrid, Spain: International Association for Shell and Spatial Structures.

Tachi, T., M. Masubuchi, and M. Iwamoto. 2012. "Rigid origami structures with vacuumatics: Geometric considerations." In *Proc., Int. Association Shell Spatial Structures-APCS*. Madrid, Spain: International Association for Shell and Spatial Structures.

Thün, G., K. Velikov, C. Ripley, L. Sauvé, and W. McGee. 2012. "Soundspheres: Resonant chamber." *Proc. ACM SIGGRAPH Art Gallery* 45 (4): 348357. https://doi.org/10.1162/LEON_a_00409.

Tyas, A., A. V. Pichugin, and M. Gilbert. 2011. "Optimum structure to carry a uniform load between pinned supports: Exact analytical solution." *Proc. R. Soc. London A* 467 (2128): 1101–1120. https://doi.org/10.1098/rspa.2010.0376.

Woodruff, J., and P. Brown. 2009. "Connecticut Science Center by César Pelli & Associates." Accessed October 10, 2016. https://www.woodruff-brown.com/.